Teleseismic P-Wave Coda Autocorrelations Versus P-Wave Receiver Functions

Michael G. Baker†, Richard C. Aster†, Derek Schutt†, Julien Chaput†, Derek Witt†

†Colorado State University

Introduction and Motivation

Auto-correlation of teleseismic P-wave coda is a recently developed technique capable of imaging crustal-scale features based on reflection signals from seismic discontinuities.[1,3]

Traditional P-wave receiver function analysis maps velocity contrasts based on P-to-S conversions and has been well utilized in a great many locations, but encounters difficulties in seismically complex environments: for example, where high impedance contrasts result in large magnitude reverberations that overwhelm the primary phases, or where high velocity layers or sloping interfaces invalidate assumptions of near-normal incidence. Deconvolution and multiple constraint alogrithms have been developed to address these issues but often introduce additional complexities and computational overhead.

Auto-correlation has the advantages of being fast (when computed via the Cross Correlation Theorem), directly exploits reverbatory phases for locating reflection horizons, and can be combined with a transformation to PSH wavevector coordinates to fully partition P- and S-wave energy into separate channels for joint inversion matching.

We present a benchmark comparison of receiver function and auto-correlation inversions utilizing data from stations with a variety of seismically complicated crustal-scale structures, including large-scale strike-sip faulting, sloping interfaces, high velocity intrusions, low velocity cratonic sediments and icecaps, and floating iceshelves.

Station	Network	Location	Years
MPAT	YT	Antarctica	'09-'12
MM27	7C	Yukon, CA	'15-'17
RS06	XH	Ross Ice Shelf	'14-'16

References

1. Phạm, T. S., & Tkalčić, H. (2017). On the feasibility and use of teleseismic P wave coda autocorrelation for mapping shallow seismic discontinuities. *Journal of Geophysical Research: Solid Earth*, *122*(5), 3776-3791.

2. Seats, K. J., Lawrence, J. F., & Prieto, G. A. (2012). Improved ambient noise correlation functions using Welch′ s method. *Geophysical Journal International*, *188*(2), 513-523.

3. Sun, W., & Kennett, B. L. N. (2016). Receiver structure from teleseisms: Autocorrelation and cross correlation. *Geophysical Research Letters*, *43*(12), 6234-6242.

4. Yu, Y., Song, J., Liu, K. H., & Gao, S. S. (2015). Determining crustal structure beneath seismic stations overlying a low-velocity sedimentary layer using receiver functions. *Journal of Geophysical Research: Solid Earth*, *120*(5), 3208-3218.

Process Flow

1) Instrument Response Removal
2) Down-Sample : 10 Hz
3) Pre-Filter : 0.4 – 1.5 Hz
4) STA/LTA : 12/7 trigger/detrigger thresholds
5) Filter : 0.2 – 0.8 Hz, using original data
6) Trim : -5 – +42 s, referenced to ak135 P-arrivals

Receiver Functions

7) Spectral Deconvolution
8) Resonance Filter[4]
9) Slowness Correction
   RFN : PmsPvms
10) Correlation Stacking
11) Final Trim : 0 – 21 s

Autocorrelations

7) Spectral Whitening[1]
   ± 10 point frequency-domain moving average
8) Welch-Method Autocorrelation[2]
   3 Segments, 50% overlap
9) Slowness Correction
   XZZ - PmpPvmp
   XRR - PmsPvms
   XZR - PmpPvms
10) Correlation Stacking
11) Final Trim : 0 – 21 s

Correlation Stacking

I use an automated method to extract only the most similar events from each station's data, as an alternative to prohibitively time-consuming manual discrimination.

For a single station, correlation coefficients, ρ, are determined for all RFN or XZZ event pairs. In the iteration, all events higher than a chosen threshold (e.g., $0.8 \cdot \rho_{max}$) are stacked non-uniquely; that is, for N events, N stacks are generated, with highly promiscuous events incorporated into multiple stacks, positively weighting those events. Subsequent iterations stack uniquely and eliminate poorly correlated, low population stacks.

Right : Results of correlation stacking of vertical channel autocorrelations (XZZ) for Antarctica station MPAT. Colored curves represent highly correlated populations of events. The black line, Σ, is the unweighted stack of all events. The 26-member stack was chosen for inversion.

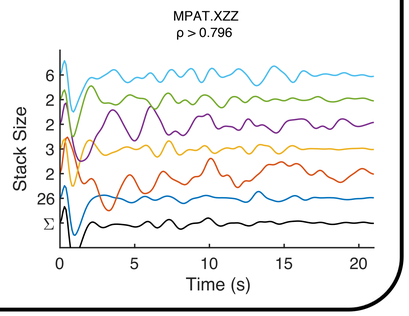

Inversion Results

Metropolis-Hastings sampled Markov Chain Monte Carlo inversions are presented below. Each model space is 13 crustal layers of variable thickness, P-wave velocity, and Poisson's ratio. Surficial layers were added where appropriate. Posterior distributions were accumulated via minimization of the least-squares misfit of the forward modeled RFN or Xxx and the observed correlated stack. XZZ, XRR, and XZR were jointly inverted, with XZZ misfits favored at a 4:1:1 ratio. Inversions ran for 500k iterations, though solutions were often determined within 30k iterations.

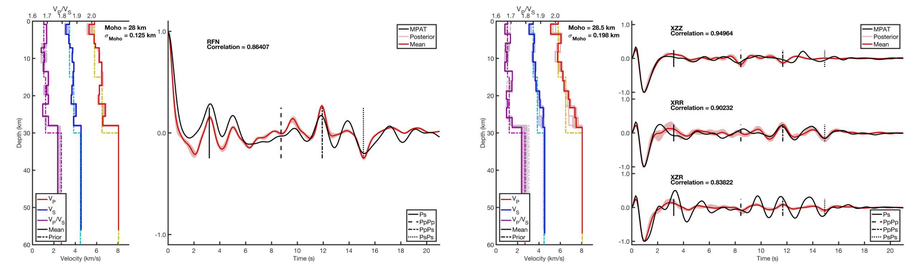

YT.MPAT, Mount Patterson, Antarctica (POLENET). This station is known for its clear Moho phases and consistent inversions and was used by this study for the initial calibration of the autocorrelation technique. The recovered 28 km Moho depth is consistent with previous studies (Chaput *et al*, 2014; Shen *et al*, 2018).

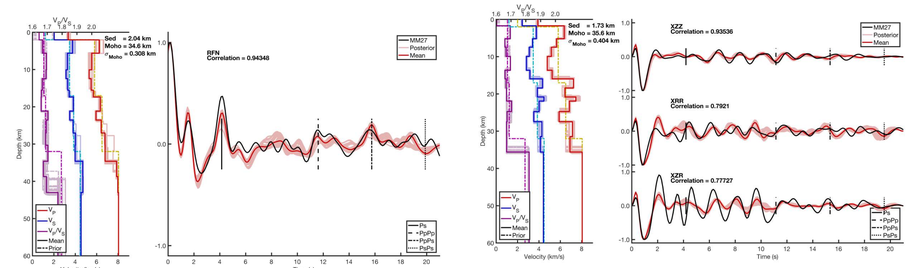

7C.MM27, Mac Pass, MacKenzie Mountains, Yukon, CA. Preliminary inversions from a currently deployed two-year campaign. Both methods find similar upper and lower crustal structures; Xxx tends towards less realistic velocity models for mid-depths. Moho depth is consistent with prior studies (Tarayoun *et al*, 2017).

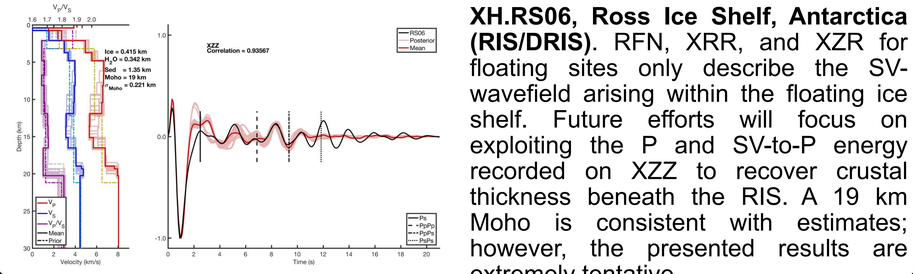

XH.RS06, Ross Ice Shelf, Antarctica (RIS/DRIS). RFN, XRR, and XZR for floating sites only describe the SV-wavefield arising within the floating ice shelf. Future efforts will focus on exploiting the P and SV-to-P energy recorded on XZZ to recover crustal thickness beneath the RIS. A 19 km Moho is consistent with estimates; however, the presented results are extremely tentative.